Fuel 185 (2016) 577–588

Contents lists available at ScienceDirect

Fuel

journal homepage: www.elsevier.com/locate/fuel

Full Length Article

Effects of pressure and preheating temperature on the laminar flame speed of methane/air and acetone/air mixtures

Yi Wu *, Vincent Modica, Bjorn Rossow, Frédéric Grisch

CORIA – UMR 6614, Normandie Université, CNRS, INSA et Université de Rouen, Campus Universitaire du Madrillet, 76800 Saint-Etienne du Rouvray, France

ARTICLE INFO

Article history:
Received 20 May 2016
Received in revised form 26 July 2016
Accepted 27 July 2016

Keywords:
Laminar flame speed
High pressure Bunsen burner
OH· chemiluminescence
OH-PLIF
Methane/air mixture
Acetone/air mixture

ABSTRACT

Laminar flame speeds of acetone/air mixtures have been investigated at elevated temperature and high pressure conditions in regards to the importance of this intermediate oxygenated molecule in hydrocarbon oxidation. Experiments were performed in an elevated pressure combustion vessel specifically designed around a concept of a premixed Bunsen flame. In a first step, measurements of the laminar flame speed of gaseous CH_4/air mixtures were performed with OH· chemiluminescence and OH-PLIF methodologies and compared with literature data in order to validate the experimental setup. The effects of the preheating temperature (373–523 K), pressure (0.1–1.0 MPa) and equivalence ratio (0.6–1.3) on the laminar flame speed of acetone/air mixtures were then examined. The experiments were finally complemented and compared with numerical simulations conducted with Cosilab commercial software package using published detailed chemical kinetic mechanisms for proposing a correlation relationship of the acetone/air laminar flame speed with pressure, temperature and equivalence ratio.

1. Introduction

With the increasingly stringent regulation of worldwide gas emissions and the need for fuels diversification, it is expected that the use of renewable fuels in the aeronautic and automotive transportation will increase. In recent years, biomass derived fuels (biofuels) have gained much attention as potential alternatives to petroleum based fuels. Apart from the advantage of renewability, biofuels have shown to be sustainable and less harmful to the environment; especially those derived from 2nd generation biofuels where sustainable lignocellulosic biomass is used as feedstock. One of the common features of biofuels is that they are all oxygenated hydrocarbons, containing oxygen as an additional element in their molecular composition. This feature distinguishes them from the hydrocarbons in conventional petroleum based fuels whose combustion chemistry has for a long time been studied. On the one hand that the use of oxygenated hydrocarbons in combustion offers significant potential for reduction in particulates and NO_x emission as compared to conventional hydrocarbon fuels. On the other hand, the incomplete combustion of oxygenated hydrocarbons may contribute to the emission of small amount of oxygenated hydrocarbons themselves or their intermediates or even harmful chemical components for environmental safety and human health. Therefore, it is crucial at the first step to understand the fundamental combustion properties of different classes of oxygenated molecules playing a key role on their formation and consumption in flames.

Laminar flame speed is one of the fundamental characteristics of the fuel/air mixtures combustion phenomena related to reaction mechanism, diffusion probability and heat release rate etc. [1–3]. It is also of practical significance in designing advanced combustion devices running at high efficiency and low NO_x emission without flashback and blow-off risks [1,2]. The present study aims to address several key issues related to the laminar flame speed of acetone which is considered as a C_3 oxygenated hydrocarbon (i.e. representing the smallest hydrocarbon regrouping alcohol isomers, aldehyde and acetone structures). This molecule has been selected as a good candidate to build a first combustion mechanism block required for the development of more accurate reaction models for larger oxygenated hydrocarbons. Acetone is also a convenient fluorescence tracer and has been extensively used in acetone PLIF technique for flow visualization and combustion study due to its photophysical advantages [4]. As a result, the chemical behavior of acetone/air mixtures as tracer on the target fuel in hot oxidizing environment must be identified to minimize its perturbation on

* Corresponding author at: CORIA – UMR 6614, Normandie Université, CNRS, INSA et Université de Rouen, Av. de l'Université, 76800 Saint-Etienne du Rouvray, France.
E-mail address: yi.wu@coria.com (Y. Wu).

http://dx.doi.org/10.1016/j.fuel.2016.07.110
0016-2361/

the target mixture and flames. Experimental measurements of laminar flame speed of acetone with high fidelity are therefore needed in operating conditions relevant to industrial burners.

An analysis of the published literature reveals that the laminar flame speed of acetone/air mixtures has been already visited by a few authors [4–10] in recent years. For instance, the fundamental physical parameters such as ignition delays, species measurements and laminar flame speed in acetone/air flames were deduced from studies performed by Pichon et al. [8]. Chong and Hochgreb [4] also performed laminar flame speed measurements using the particle imaging velocimetry (PIV) optical technique in a jet-wall stagnation flame at atmospheric pressure and for an inlet temperature of 300 K. In the most recent study by Nilsson et al. [7], acetone/air laminar flame speeds were measured using a perforate plate burner at atmospheric pressure, and the initial fuel/air mixture temperature range was extended for the first time to higher values from 298 to 358 K. However, large discrepancies between laminar flame speeds were observed from these experimental investigations. By comparing previous experimental results of acetone/air mixture at 298 K and atmospheric pressure conditions it was found that the gap between previous measurements could be up to 40% [4–8]. Furthermore, few experimental investigations at larger pressure and preheating temperatures >400 K are displayed in literature. As a consequence, for a better understanding of the acetone combustion process, it is necessary to complete these acetone/air flame studies over much wider temperature, pressure and equivalence ratio ranges.

By definition, the laminar flame speed, S_u, is the velocity relative to the unburned gas in which a planar, one-dimensional flame front travels along the normal to its surface [11]. The main experimental methods for measuring laminar flame speeds involve stretched (counter flow or stagnation) [12–15], spherical time-varying (spherical bomb) [16–21], curved (Bunsen type) flame [1–2,22–28] and heat flux method [3,7,29–30]. Each of these approaches has its own advantages and range of applicability. For instance, the advantage of spherical bomb method is the capability to perform high pressure measurements; meanwhile one of its main drawbacks is the difficulty in measuring flame speed at relatively high reactive temperature. At high temperature, the auto-ignition time of the reactants is reduced and can be comparable to the residence time required to ensure no motion of the reactants in the combustion chamber. The counter flow method needs extrapolation to zero stretch and this technique is not adapted for reactive mixtures featuring high burning velocity. The heat flux method are considered as a promising method as the flame is quasi-adiabatic and flat, thus a direct determination of the laminar flame speed is possible without correction for stretch. However, the heat flux method has a limitation in measured velocity, so that S_u up to 40–70 $cm.s^{-1}$ can be measured, and above that, the flame area becomes disturbed by the presence of the perforated burner plated. Premixed Bunsen flame has been one of the pioneer investigated flames in the past. The Bunsen flame is controlled by rather complicated physical phenomena and the main disadvantages include modifications due to heat losses at the rim of the nozzle, variable stretch and curvature effects on the flame tip and potential modifications of the equivalence ratio of the fuel/air mixture due to fresh air entrainment around the flame [27,31]. Nevertheless, the same as the other measurements methods Bunsen flame experimental configuration are still be used recently as it offers attractive properties to measure laminar flame speeds in regards to its simplicity to study fuel/air mixtures with variable preheated temperature and elevated pressure conditions. Furthermore, the combination of this type of burner and an additional controlled evaporator and mixer system may help to achieve vaporized large molecule weight liquid fuels/air mixtures. In the recent work by Wang et al. [2], comparisons between OH-PLIF Bunsen flame method and heat flux method were performed by measuring laminar flame speed of syngas/air mixtures at the same measurements conditions. It is found that the flame speeds measured by attentively employed Bunsen flame method can be closed to the adiabatic laminar burning velocity measured by heat flux method. More recently, by using Bunsen flame method Gao et al. [28]investigated the effect of ozone addition on laminar flame speed of syngas/air mixtures in low and moderate pressure conditions. Sun et al. [32] measured flame speed of $CO/H_2/O_2/H_2$ mixtures using Bunsen flame method to validate new developed chemical mechanisms. A summary of available experimental investigations inthe last ten years on laminar flame speed measurements using Bunsen flame is given in Table 1. According to the literature, simple gaseous fuels are mostly often used to perform laminar flame speed measurements in Bunsen flames at atmospheric pressure. Unfortunately, applications of Bunsen burners for studying complex fuels such as vaporized liquid fuels at elevated pressure and preheating temperature conditions are still limited. In the current work, the Bunsen flame concept is optimized to perform laminar flame speed measurements of vaporized acetone fuel at various preheating temperatures in elevated pressure environments (up to 1.0 MPa).

The structure of this paper is described as follows. First of all, a new high-pressure laminar flame burner has been designed for monitoring laminar flames of gaseous or liquid fuels over a wide range of operating conditions including preheating temperature, pressure and equivalence ratio. The high pressure combustion chamber, fuel vaporization system and optical diagnostic systems are presented indetail in Section 2. The experimental methodology used for the measurement of the laminar flame speed is then described in Section 3. The error sources associated to these techniques are discussed and a new image processing method is proposed. The numerical results are presented and discussed in Section 4. Measurements of the laminar flame speed at high pressure for primary reference CH_4 fuel are firstly presented to validate the high-pressure Bunsen burner and to complement experimental data published in the literature. Then the experimental work is extended to the measurements of the laminar flame speed of acetone/air mixtures at pressure ranging between 0.1 and 1.0 MPa, temperature of 373–550 K and equivalence ratio of 0.6 to 1.3. A comparison between these measurements and numerical simulation using a detailed chemical mechanism is finally accomplished. The last section is devoted to provide improved empirical correlation for laminar acetone/air flames, as well as to study their temperature and pressure dependencies. For this purpose, an analysis of the effects of pressure, temperature and equivalence ratio on the laminar flame speed and an empirical flame speed correlation in function of these parameters are proposed.

2. Experimental details

2.1. High-pressure Bunsen burner

The burner assembly and pressure chamber used to produce the high-pressure combustion are illustrated in Fig. 1. The chamber is designed to burn up to 3.0 MPa at a maximum wall temperature of 600 K. An axisymmetric premixed burner is designed and developed to generate a steady conical laminar premixed flame stabilized on the outlet of a contoured nozzle in a high pressure chamber (Fig. 1). The shape of the axisymmetric central contracting nozzle is designed with a fifth-order polynomial to reduce the boundary layer thicknesses by accelerating the flow and providing a flat velocity profile at the nozzle outlet. The contoured nozzle has an outlet diameter of d_1 = 10 mm and a contraction ratio of $\delta = (D/d_1)^2 = 49$. A second concentric contoured nozzle of outlet diameter of d_2 = 10.6 mm surrounding the central nozzle

Table 1
Overview of laminar flame speed measurements using Bunsen flame in literature.

Year	Author	Ref.	Optical technique	P (MPa)	T (K)	Fuel
2006	Dagaut et al.	[51]	Chemiluminescence	0.1	480 K	Kerosene
2007	Natarajan et al.	[26]	Chemiluminescence	0.1	300 K	H_2/CO
2009	Dong et al.	[1]	Chemiluminescence	0.1	300 K	H_2/CO
2010	Mazas et al.	[25]	Schlieren	0.1	373 K	CH_4/H_2O
2011	Selle et al.	[31]	Chemiluminescence	0.1	300 K	CH_4 /H_2O
2011	Burbano et al.	[23]	Schlieren	<0.1	300 K	H_2/CO
2011	Bouvet et al.	[22]	Chemiluminescence	0.1	300 K	H_2/CO
2012	He et al.	[52]	OH-PLIF	0.1	300 K	H_2
2013	Fu et al.	[53]	OH-PLIF	0.1	300 K	H_2/CO
2013	Lapalme et al.	[54]	Chemiluminescence	0.1	295–450 K	H_2/CO
2014	Hu et al.	[55]	Chemiluminescence	0.1	300 K	CH_4/O_2/CO_2
2015	Wang et al.	[2]	OH-PLIF	0.1	300 K	H_2/CO
2015	Gao et al.	[28]	Chemiluminescence	0.025–0.3	300 K	CH_4/C_2H_4/C_3H_8/O
2016	Sun et al.	[32]	Chemiluminescence	0.1	300 K	CO/H_2/O_2/H_2O

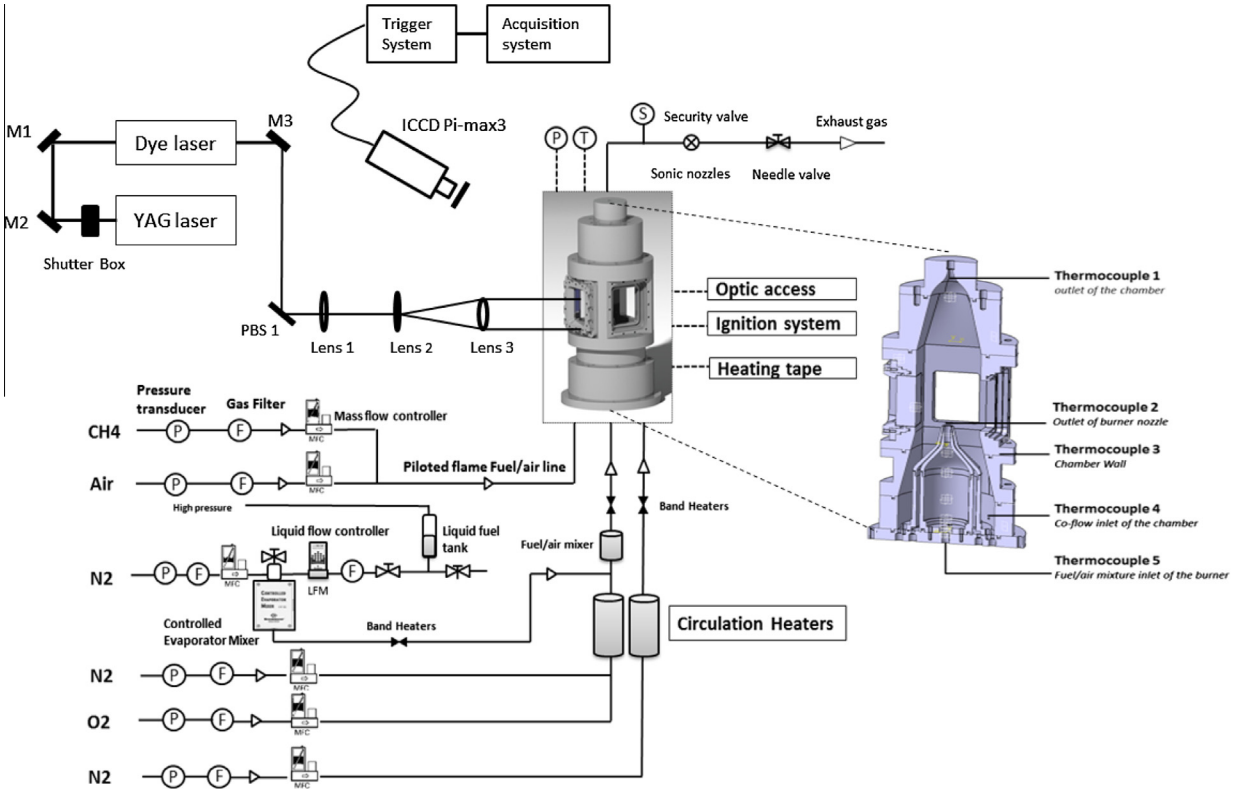

Fig. 1. Experimental set-up.

is used to produce a flat, fuel/air pilot flame to anchor the conical laminar premixed flame in high pressure operating conditions. Both nozzles are mounted on the bottom flange of the pressure chamber as well as a guard-flow housing located between the walls of the second nozzle and the pressure chamber. The high-pressure chamber, constructed in stainless steel has an inner surface of 100 × 100 mm^2 and a height of 511 mm. It is equipped with four large UV quartz optical windows tailored to probe the flame with optical imaging diagnostics. The preheating of the pressure chamber is performed using electrical wire heaters positioned around its external surface (Fig. 1). Five type K thermocouples are placed at different positions of the pressure chamber to monitor and ensure temperature uniformity throughout the pressure vessel while the chamber pressure is monitored with a piezoelectric transducer. The top of the pressure chamber is designed as a convergent nozzle adopting a contraction ratio of 100 along a length of 160 mm and a honeycomb plate is placed on the top of the vessel as a flow straighter to suppress the presence of large circulation zones inside the pressure chamber.

2.2. Liquid fuel vaporization and gas feeding

For these experiments, the burner can operate with gaseous or liquid fuels. Liquid fuel was pressurized in a 1.0 L tank and nitrogen and oxygen were supplied by pressurized tanks. The oxygen and nitrogen flowrates are regulated by an electronics unit connected to the different mass flow controllers, previously calibrated with the related gases. For liquid fuels, the 1.0 L tank is connected to liquid flowmeter associated with a Controlled Evaporator and Mixer (CEM, Bronkhorst) which heats and mixes fuel vapor with N_2 carrier gas at controlled mass flowrate and temperature. The exit of the CEM is connected to a stainless steel mixing cell preheated at temperature ranging from 373 to 600 K and controlled with a type K thermocouple to prevent any condensation of the fuel vapor.

Additional nitrogen and oxygen initially mixed and preheated by a circulation heater before the entrance of the mixing cell are used to reproduce the synthetic species composition of air and to modify the equivalence ratio of the heated fuel vapor/air mixture. In the present study for acetone/air mixtures measurements, air is assumed to be a gaseous O_2/N_2 mixture with a volume ratio of 20/80. For CH_4/air mixtures measurements, as there is no need of the vaporization system the reacting mixture is obtained directly by mixing CH_4 and air with compositions (O_2/N_2 volume ratio of 21/79). As the measurement accuracy of the laminar flame speed S_u is sensitive to the flame stability, the vaporized fuel/air mixture is injected into the central nozzle which is filled with high-temperature resistant glass beads (1–3 mm diameter) to prevent any flow inhomogeneity at the nozzle exit. The same strategy is also applied for the fuel/air mixture required for the pilot flame as well as for the nitrogen guard-flow. The annular nitrogen guard flow is used to adjust the pressure in the vessel and to dilute the exhaust gases. The annular nitrogen guard-flow is first preheated by a circulation heater and then delivered to the pressure vessel by a combination of four rigid stainless steel tubes (4 mm i.d.) connected to the bottom flange of the vessel. The combustion reactants (gaseous methane and air) devoted to feed the pilot flame are delivered to the burner by two rigid stainless steel tubing. A T-connection of both tubes is then achieved to mix methane with air before their injection inside the burner via a set of four tubes rigid stainless steel tubes connected to the bottom flange of the vessel. To minimize the effect of the pilot flame on possible disturbances on the main flame, the flowrate of the fuel/air mixture for the pilot flame is kept as low as reasonably achievable. In the case of CH_4/air flames, the equivalence ratio of the piloted flame is kept the same as the equivalence ratio of the central flame and in the case of acetone/air flames, the equivalence ratio of the piloted flame is fixed to the value $\varphi = 1.2$ for all the operating conditions studied.

Combustion products are finally evacuated and cooled through rigid stainless steel tubing connected to the top of the pressure vessel. This tubing is then split into four channels, including, respectively, sonic throats of 0.5, 0.7, 1.0 and 1.1 mm internal diameters. The increase in pressure was achieved in several steps by successively closing each of the sonic throats. High-pressure flames are obtained by using the following procedures: (1) the flame is ignited at 0.1 MPa using an igniter, (2) the flow rates of fuel/air mixtures are adjusted to achieve a stable flame at a fixed equivalence ratio; (3) the flowrate of nitrogen guard-flow is adjusted to achieve a flow velocity ratio with the fuel/air mixture of about 1/10; (4) the nitrogen guard-flow and fuel/air mixture flowrates are then increased proportionally to increase the pressure slowly and to prevent the flame from flash back.

2.3. Optical diagnostics

2.3.1. OH· chemiluminescence

One of the optical techniques used in the current study is based on the flame contours detection by using the OH· chemiluminescence image technique. The camera used to record the OH· radical emission is a thermoelectrically cooled, 16-bit intensified CCD camera (PI-MAX 3, Roper Scientific) with a 1024×1024 array. The camera is equipped with a f/2.8, f = 100 mm, achromatic UV lens (CERCO) combined with a short pass optical filter centered at 310 nm and having a bandwidth of 10 nm. The exposure time selected to record the OH· emission image is defined by opening the intensifier gate at 1 μs. A 40×40 mm^2 area of the flame is imaged by the ICCD camera, so that the spatial resolution is about 40 μm per pixel. The acquisition repetition rate of the camera is kept at 10 Hz.

2.3.2. OH-PLIF

The OH planar laser-induced fluorescence laser diagnostic (OH-PLIF) used in the current work consists of a cluster of a Nd:YAG laser (Quanta-Ray Pro-190), dye laser (Sirah PRSC-G-3000) and high resolution ICCD camera (PI-MAX 3, Roper Scientific). A frequency-doubled, Q-switched Nd:YAG laser was used to pump a dye laser, which was then frequency doubled to obtain wavelengths in the 280–290 nm spectral range. The dye laser was tuned to 282.75 nm to excite the Q_1 (5) line of the (1, 0) band of the OH ($X^2\Pi$ - $A^2\Sigma^+$) system. The UV laser beam at the exit of the laser source is transported via optical mirrors around the burner. It is transformed into one collimated sheet of 50 mm large using a set of converging and divergent cylindrical lenses and a spherical lens. The two cylindrical lenses form a telescope which spreads the beam into a collimated sheet. Only the central zone of the laser sheet (one third) is used for our experiments in order to obtain a laser sheet energy profile as flat as possible. This methodology, allows, in a first assumption, a good proportionality between the fluorescence signals and the probe fluorescent species concentration. Laser energy was fixed at 5 mJ to maintain the fluorescence of OH radical within the linear regime in order to keep the proportionality between the OH fluorescence signal and the OH concentration. Fluorescence images were recorded with a 16-bit, 1024×1024 pixels, ICCD camera with an intensifier gate width of 1 μs and a framing rate of 10 Hz. The camera is equipped with the same optical lens and optical filters as for the OH· chemiluminescence technique. Examples of OH· chemiluminescence and OH-PLIF images are displayed in Fig. 2 in case of methane/air flames operating with equivalence ratio 0.7, 1.0 and 1.3.

3. Laminar flame speed measurement

3.1. Flame speed determination method

The principle of laminar flame speed measurements is based on the mass conservation between the outlet nozzle and the flame front. The average flame velocity in the transverse plane is expressed by:

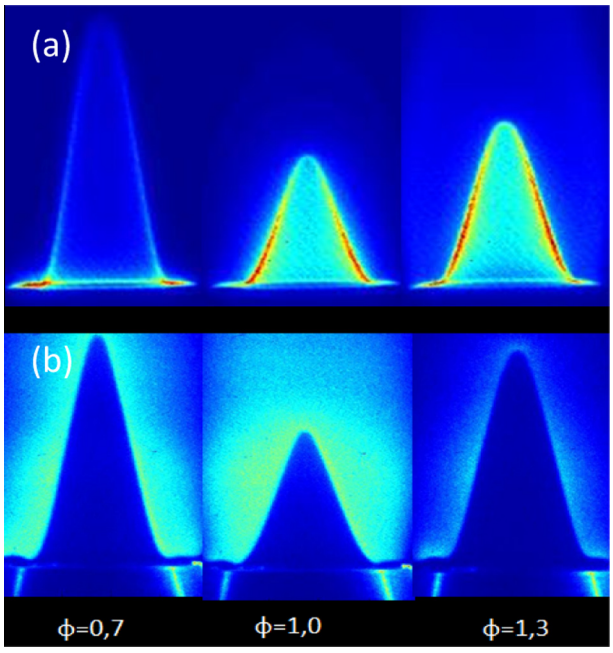

Fig. 2. Methane/air flames for various equivalence ratios: (a) OH· chemiluminescence images (T = 300 K, P = 0.1 MPa); (b): OH-PLIF images (T = 373 K, P = 0.1 MPa).

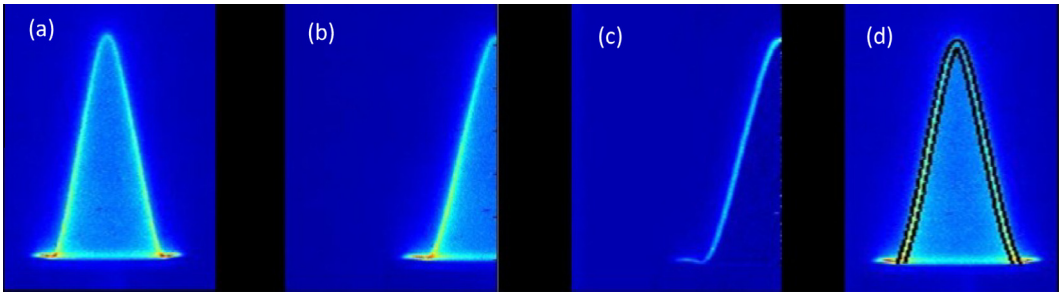

Fig. 3. OH· chemiluminescence image processing: (a) original OH· chemiluminescence image, (b) division of the image in two parts, (c) Abel-inverted image, (d) unburned gas contours detection with flame thickness consideration.

$$\rho_u S_u A = Q_m \rightarrow S_u = Q_m/(\rho_u A) \quad (1)$$

where Q_m is the total mass flow rate of the fuel/air gaseous mixture, ρ_u is the unburned gas density and A is the surface area at the reaction zone of the flame. The surface area A is determined from the flame structure observed on the OH· chemiluminescence images. The methodology selected to process the OH· emission images is then illustrated in Fig. 3. The location of the maximum intensity contours of OH· emission is firstly detected with an image processing algorithm based on the inverse Abel transformation. This method, used as a way of converting line-of-sight integral projection data of an axisymmetric measurement field into a spatially resolved field distribution is written using the Matlab formalism. Since the laminar flame speed is relative to the unburned reactive gaseous mixture and not the zone in which the OH concentration into the flame is maximal, the flame front area *A* is then defined as the upstream boundary of the preheating zone of the fresh gases. As this boundary can be different from the maximum OH· contours (see Fig. 4), the determination of the location of the upstream boundary of the preheating zone is processed using the following method. The location of the flame front area A is determined by isolating on the OH· chemiluminescence images the zone in which the OH· signal is maximum. Then, using 1D adiabatic premixed flame simulation with the Cosilab software permits determination of the temperature profile and the OH radical changes through the flame wave. Hereby as the flame is laminar, assumption was made that OH· and OH radicals follow similar spatial profiles and reach a maximum concentration at the same locations [33]. The theoretical "flame thickness δ" is calculated as the distance separating the isotherm T = 800 K in which OH· begins to be experimentally detected using optical diagnostics and the frontier in which the theoretical OH concentration is maximum. From these values, the position of the contour of the flame front is then defined as the position of the maximum OH· contour minored by δ. Once the contour of flame front is determined (as shown in Fig. 4, the blue one)[1], the flame area is calculated by pivoting this flame contour profile f(x) along the burner axis using the Eq. (2):

$$A = 2\pi \int_a^b f(x)\sqrt{1 + [f'(x)]^2}\,dx \quad (2)$$

where a and b are the boundary limits of integration. f(x) is the flame contour profile obtained by image processing.

Fig. 5 displays the evolution of the flame thickness of acetone/air flames versus pressure for T = 473 K and φ = 1.2. An observation of this figure reveals that the flame becomes much thinner as the level of pressure increases. The influence of the pressure on the flame thickness is drastic at lower pressure but reduced at elevated pressures. The maximum value of δ, equal to 0.75 mm at atmospheric pressure is continuously decreasing when the pressure increases up to 0.5 MPa. For P > 0.7 MPa, the flame thickness is finally reduced to 0.1 mm. These results indicate that a flame thickness correction on the position of the surface A should be carried out especially for pressures blow 0.7 MPa. Beyond this pressure, the maximum OH· contours can be assumed to be representative of the preheating zone boundary in regards to our experimental spatial resolution adopted in the current work. This observation is confirmed from OH-PLIF measurements which will be discussed in Section 5.

Furthermore, as theflame is conical in shape and not one-dimensional (1D), the importance of the flame stretch effect on behalf of the aerodynamic strain and flame curvature on the laminar flame speed measurements has to be evaluated [34]. As the geometry of the nozzle was designed to minimize the boundary layer thicknesses, the velocity profile at the nozzle exit is flat enough that the aerodynamic strain is thus limited. Concerning the flame curvature effect, the condition involving a constant burning velocity on the surface area of the flame front is evidently not respected. For instance, Fig. 6 shows the evolution of the flame structure recorded at various levels of pressure. Temperature and equivalence ratio are fixed to 473 K and 0.8 respectively. As observed on the OH· images, the region in which a flame curvature is noted is only visible at the tip of the flame. To estimate the importance of its surface area on the surface area of the flame front, the evolution of the curvature rate with the radius of the flame is then plotted for various pressures (Fig. 6). It is found that the flame curvature becomes smaller and sharper when the pressure increases. In elevated pressure conditions, the flame structure becomes similar as a straight edge triangle flame; a curvature gradient appears at the tip of the flame in a smaller region that significantly reduces the magnitude of the flame curvature on the measurement of the laminar flame speed. From measurements, the maximal magnitude of the surface of the flame curvature represents only ~2% of the whole surface area of the flame front. In considering this value comparable to the accuracy of our laminar flame speed measurements, the flame stretch effect could be disregarded [25,35]. Nevertheless, it should be noted as the streamlines approaching the flame surface have to be bent according to the flame angle, the laminar flame speeds must be different from adiabatic unstreched flame speeds. In the current work, the laminar flame speeds measured are strictly Su since stretch effects are not taken into account as compared to the counterflow or spherical expanding flames in which S_U^0, corresponding to the unstreched laminar flame speed, can be measured. Fortunately, the differences between both values can be negligible in our experiments in regards to results presented in Refs. [26,35], showing good similarities between Su and S_U^0 in premixed Bunsen flames.

3.2. Data acquisition and uncertainty estimate

For both OH· chemiluminescence and OH-PLIF measurements, 30 instantaneous images are systematically recorded and the

[1] For interpretation of color in Fig. 4, the reader is referred to the web version of this article.

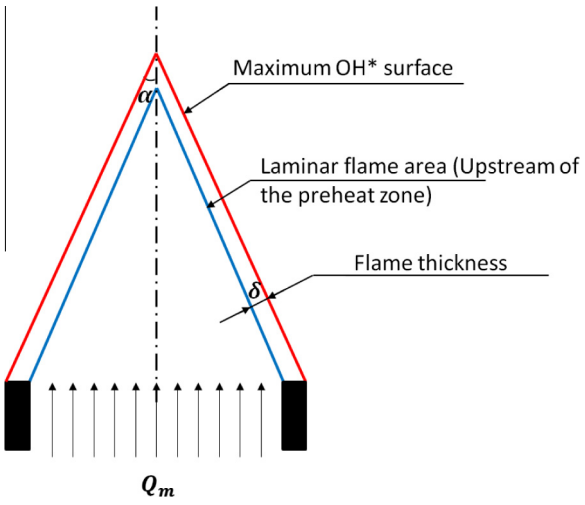

Fig. 4. Determination of the flame surface area.

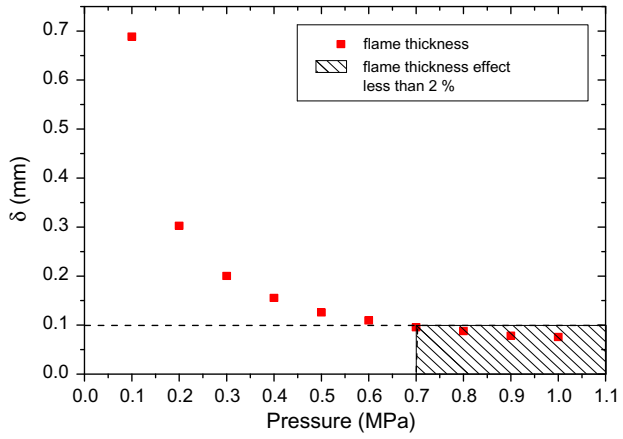

Fig. 5. Evolution of the numerical flame thickness with pressure (acetone/air mixture, T = 473 K, P = 0.1–1.0 MPa, φ = 1.0).

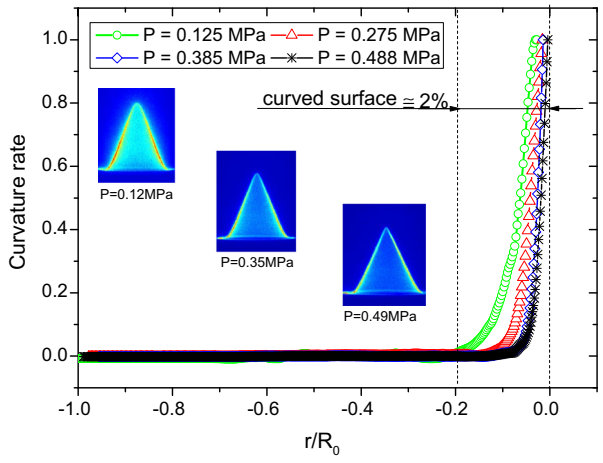

Fig. 6. Normalized flame curvature rate along radius axis for various pressures (T = 473 K, φ = 0.8). Burner rim starts at $r/R_0 = -1$ and burner center position is at $r/R_0 = 0$ with a burner radius $R_0 = 5$ mm.

resulting laminar flame speed is determined by data processing of averaged images deduced from the set of the instantaneous images.

The uncertainty of the measured flame speed is estimated from two main sources: the uncertainty of the total flow rate of unburned gas (U_{Qm}) and the uncertainty of the calculated flame area (U_A). U_{Qm} comes from the mass flow controller uncertainty (0.5% of reading + 0.1% full scale) which is estimated to be ~2% and U_A derives from the camera spatial resolution which is estimated to be ~3%. The overall uncertainty is calculated from the relation $\sqrt{U_{Qm}^2 + U_A^2}$ and is equal to ~4% for all the laminar flame speeds that are recorded at a temperature range of 300–523 K, an equivalence ratio range of 0.6–1.3 and at ambient pressure. As an example, for all these experimental conditions the uncertainty varies from ±1 cm/s (300 K, 0.1 MPa) up to ±4 cm/s (523 K, 0.1 MPa).

It can be noted that this order of magnitude is also valid in case of higher pressure (up to 1 MPa) for lean flames but it increases in case of rich flames. Indeed, another major source of uncertainty is related to the limited range of stable flame regime for high pressure rich flames which amplifies up to ~7% the overall uncertainty in values of S_u. In the most unfavourable case of this study (acetone/air mixture at 0.35 MPa, 473 K and φ = 1.2), the highest uncertainty of S_u is estimated to be around ±4.5 cm/s.

The uncertainties in equivalence ratio are also estimated for each experimental condition and they are calculated from the mass flow controller uncertainty. The uncertainty in equivalence ratio is less than ~3% for methane/air mixture and less than ~1% for acetone/air mixture.

4. Numerical method

The Cosilab commercial software package including full transport properties is used to calculate one-dimensional laminar flames of methane/air and acetone/air for various equivalence ratios, preheating temperatures and pressures. The transport properties are deduced by using the mixture averaged diffusion model. The Newton unsteady adaptive mesh algorithm has been used and allows an adaptive mesh refinement during the computation ("grad" and "curve" values are fixed to 1×10^{-5}). The total final number of the grid points is 200 for a physical domain of 0.1 m in order to ensure a chemical equilibrium state in the burned gases. The number of grid was proved to be sufficient to make the simulated results grid-independent. Methane/air flames are modelled using the establish GRI-Mech 3.0 chemical mechanism [36]. It consists of 325 elementary chemical reactions with associated reaction rate coefficients and thermochemical properties for the 53 species involved. Acetone/air flames are modelled using a sub-mechanism added to GRI-Mech 3.0 which has been initially developed by Pichon et al. [8] and recently modified by Chong and Hochgreb [4]. This modified GRI-Mech 3.0 mechanism is extended with acetone oxidation and pyrolysis reactions and it involves 81 species and 419 reversible reactions.

5. Results analysis

Preliminary experiments were first conducted with methane/air mixtures in order to validate the high-pressure Bunsen burner, the optical diagnostics and the post-processing technique in various operating conditions including variations of equivalence ratio, temperature and pressure. Then in order to illustrate the preheating temperature effect on the acetone/air laminar flame speed, experimental measurements are performed firstly at atmospheric pressure condition with different temperatures: 373 K, 403 K, 443 K, 468 K and 523 K. Laminar flame speed measurements are subsequently performed at high pressures from 0.1 to 1.0 MPa with equivalence ratios ranging from 0.7 to 1.2. For high pressure measurements, the preheat temperature is fixed at T = 473 K. The

experimental operating conditions investigated for high pressure measurements of acetone/air mixtures are listed Table 2.

5.1. Correlation description

One of the objectives of this work is to provide a general expression for an empirical correlation of the laminar flame speed of acetone/air mixtures, validated for a large range of equivalence ratio φ, temperature T and pressure P. Indeed, it seems to the authors' knowledge that for acetone/air flames the pressure dependency on the flame speed has only been investigated by few previous works and at limited pressure ranges. As already known, laminar burning velocity is a strongly dependent parameter of mixture features, e.g. preheating temperature, pressure and mixture equivalence ratio. And generally, this fundamental parameter is determined at standard temperature and pressure conditions or at relatively low temperature and pressure, primarily owing to difficulties in the operating of the experimental setups and measurements. However, in practical applications, initial conditions of pressure and temperature of the fuel/air mixture are often larger than the standard values. Therefore, it is very important to quantify the effects of pressure and temperature on this fundamental parameter [37]. According to literature, several empirical temperature and pressure dependency correlation expressions can be found in previous laminar flame speed investigations [38–40]. One of the frequently used temperature and pressure dependence correlations is the power-law:

$$S_u = S_{u0}(T/T_0)^{\alpha}(P/P_0)^{\beta} \quad (3)$$

In this formula, the laminar flame speed, $S_{u0,}$ is expressed at reference conditions of temperature (T_0) and atmospheric pressure (P_0) and is multiplied by correction factors displaying the temperature and pressure dependencies. This relation has been used and validated by various previous investigations. For instance, Metghalchi and Keck [38] proposed this correlation by flame speed measurements of isooctane/air mixtures in the temperature range 298–700 K and the pressure range 0.04–0.5 MPa. In this study, Metghalchi determined laminar burning velocities from the pressure rise of explosions in a spherical bomb. Gülder [41] validated this empirical formula by measuring the propagation of ethanol/air spherical flames over a preheating temperature ranging from 300 to 500 K and at pressure up to 0.8 MPa. In the study of Varea et al. [16] using the spherical bomb method, the pressure dependency correlation is completed by introducing the effect of the fuel blending. Generally speaking, the main factor that determines the credibility of these interpolations is the accurate experimental measurements validation over the largest possible range of working conditions.

In the present study the aforementioned power-law correlation is used as represented by Eq. (3). The effect of the equivalence ratio on Su_0 is taken into account in Eq. (4) by using an extended formulation of Metghalchi and Keck [38].

$$S_{u0}(\varphi) = S_{u_0,\varphi=1} + S_{u_0,1}(\varphi-1) + S_{u_0,2}(\varphi-1)^2 + S_{u_0,3}(\varphi-1)^3 + S_{u_0,4}(\varphi-1)^4 \quad (4)$$

where $S_{u_0,\varphi=1}$ is the laminar flame speed at φ = 1 and $S_{u_0,i}$ the parameters to be determined for initial temperature T_0 of 373 K and pressure P_0 of 0.1 MPa.

It is widely held view that the power exponents α and β depend on the equivalence ratio [38,41]; they can be expressed by the following polynomial relations:

$$\alpha(\varphi) = \alpha_0 + \alpha_1(\varphi-1) + \alpha_2(\varphi-1)^2 + \alpha_3(\varphi-1)^3 \quad (5)$$

$$\beta(\varphi) = \beta_1 + \beta_2(\varphi-1) + \beta_3(\varphi-1)^2 \quad (6)$$

Table 2
Experimental conditions of pressure and equivalence ratio for laminar flame speed measurements of acetone/air mixture at T = 473 K.

Equivalence ratio φ	Pressure (MPa)
0.7	0.1–0.75
0.8	0.1–1.0
0.9	0.1–0.65
1.0	0.1–0.45
1.1	0.1–0.45
1.2	0.1–0.35

The parameters $S_{u0}(\varphi)$, α and β were determined from laminar flame speed measurements for the following ranges of experimental conditions: $0.6 \leqslant \varphi \leqslant 1.3$, $373 \leqslant T \leqslant 523$ K, $0.1 \leqslant P \leqslant 1$ MPa. Their values and the thermodynamic effects on the acetone/air flame speed are presented in the next sections.

5.2. Methane/air mixture

5.2.1. Pilot flame effect

The effect of the pilot flame on the laminar flame speed measurements was estimated by comparing measurements of laminar flame speed recorded from atmospheric CH_4/air flames assisted with and without the pilot flame. For instance, Fig. 7 depicts a comparison of the evolution of the laminar flame speeds with the equivalence ratio. Measurements are performed with a preheating temperature of 375 K. An observation of the results reveals tiny differences between the laminar flame speeds, i.e. 0.5–1 cm/s at φ = 1. Although this deviation represents ~2% variation of the laminar flame speed, both values remain within the experimental uncertainty delivered from the data processing of the OH· chemiluminescence images. Moreover, this deviation has a tendency to come down for higher preheating temperature conditions because of the increase of the laminar flame speed. The same tendencies also observed for the laminar flame speed measurements of acetone/air mixtures enable us to disregard the influence of the pilot flame in the current study.

5.2.2. Influence of the flame thickness correction

As aforementioned, the accuracy of the laminar flame speed measurements from a Bunsen flame mainly depends how the surface area of the flame front is determined. From the OH· chemiluminescence images, the laminar flame speed is commonly defined by the fresh gas boundary layer that perhaps does not coincide with the position in which the OH· signal is maximum. That position requires to be reduced by taking into account the flame thickness. To test the accuracy of this method, the laminar flame speeds deduced from the OH· chemiluminescence images are compared with those measured from the OH-PLIF images. Based on the fluorescence images, the location of the flame surface area is defined as the inner frontier for which the OH signal begins to be detected. This statement is validated because it corresponds to the thin region in which the chemical reactions as well as a sharp gradient of temperature occur. Fig. 8 displays the evolution of the laminar flame speed with pressure 0.1–1.0 MPa, both recorded with OH-PLIF and OH· chemiluminescence techniques. Measurements are performed for a preheating temperature of 473 K and an equivalence ratio of 1.2. Also shown on the figure are the results of the GRI-Mech 3.0 prediction. In a general way, the experimental results show particularly good agreement when compared to the GRI- Mech 3.0 simulations. For each technique, the laminar flame speeds decrease nearly logarithmically with pressure. It can be also shown in Fig. 8 that the OH· chemiluminescence measurements corrected with the flame thickness are in well accordance with the OH-PLIF measurements and the GRI-3.0 predictions. On the

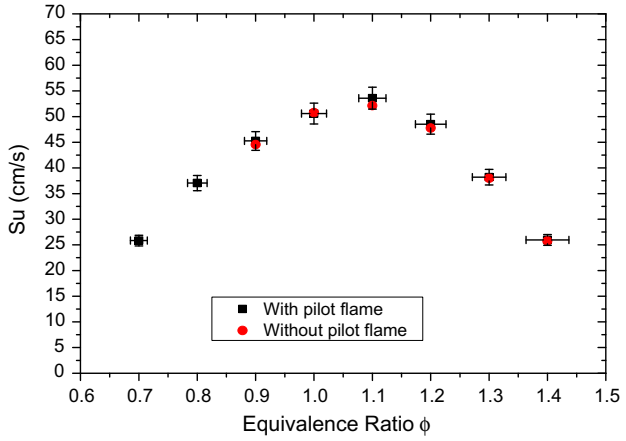

Fig. 7. Pilot flame effect on the laminar flame speed measurements (CH_4/air mixture, T = 375 K, P = 0.1 MPa).

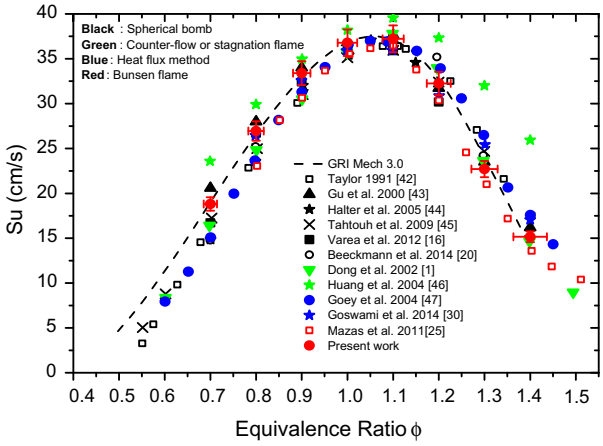

Fig. 9. Laminar flame speed comparison between experimental measurements, literature results and simulated results using GRI-Mech 3.0 (CH_4/air mixture, T = 300 K, P = 0.1 MPa).

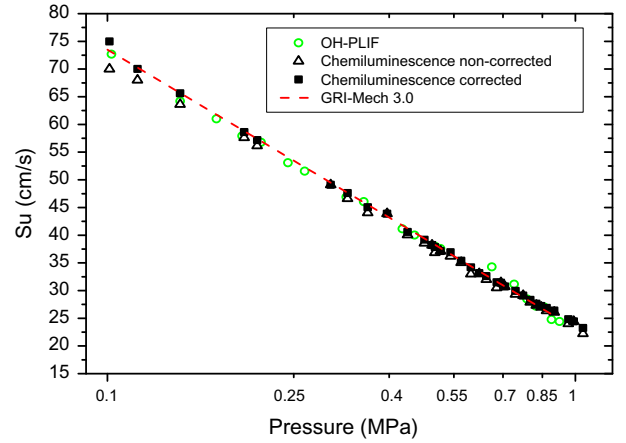

Fig. 8. Relationship between laminar flame speed and pressure (CH_4/air mixture, φ = 1.2, T = 473 K). Comparison between OH· chemiluminescence and OH-PLIF methodologies.

contrary, the uncorrected OH· chemiluminescence signals underestimate the laminar flame speeds especially for lower pressures. For elevated pressures, the difference between corrected and uncorrected values vanishes in regards to the large decrease of the flame thickness with pressure (see Fig. 5). According to these results and the ease of use of the OH· chemiluminescence technique, the laminar flame speed measurements presented in the following sections have been accomplished with this optical diagnostic. For the current work, the flame thickness used to correct the OH· chemiluminescence signals is calculated for methane/air mixtures with the GRI-Mech 3.0 kinetic mechanism [36] while the detailed kinetic mechanism of Chong is used for determining the flame thickness of acetone/air mixtures [4].

5.2.3. Equivalence ratio effect

As a means of validating the current measurement approach, Fig. 9 shows a comparison of the laminar flame speed results obtained with the different experimental approaches for a CH_4/air mixture at 300 K and at 0.1 MPa. Laminar flame speeds which are measured in this current work are compared to spherical bomb flame speeds [16,20,42–45], stretch-corrected flame speeds from counter flow and stagnation flames [14,46], flamespeed obtained with the heat flux method [29,47] and flames speeds measured on a conical flame [25]. In addition, Fig. 9 also shows the GRI-Mech 3.0 prediction. For all these flames speeds results, the data scattering is up to ±8 cm/s at lean and rich side and of ±3 cm/s at approaching stoichiometric condition. With the exception of the results of Huang et al. [46] and those of Mazas et al. [25] that depict large discrepancies, the overall agreement among the data is generally good, with a better agreement between the current data and the GRI-Mech 3.0 prediction. For equivalence ratios between 0.55 and 0.7, almost all measurements identified in the literature give underestimated values compared to the results of the simulation. The experimental results, however present a better accordance with simulations for φ > 0.7. Interestingly, it is observed that the results obtained with the spherical bomb technique as well as the heat flux method have the tendency to underestimate the simulations in the lean regime side and overestimate in the richer side. The counter-flow flame or stagnation flame methods generally overestimate the laminar flame speeds. Compared with these measurements techniques, the heat flux method appear to gives less data scattering than the others type of measurements. For the present work, laminar flame speeds which are obtained using the flame thickness correction have a good agreement with GRI prediction and they are located in the intermediate part of previous scattering data.

5.2.4. Preheating temperature effect

To explore the sensitivity to the preheating of the reactants, comparisons of measured and simulated laminar flame speeds for atmospheric pressure and for various preheating temperatures are presented in Fig. 10. The temperatures investigated are 300 K, 375 K, 418 K and 477 K respectively. For low temperature cases (300–400 K), the simulation produces a fairly close approximation of the measurements, which should help to assure the reader that the simulation results presented thus far provide a reasonably accurate representation of methane/air flame speeds. For higher reactant temperatures (T > 400 K), the GRI prediction provides a less accurate match to the data, especially for φ > 1, but qualitatively the results are similar. This is accordance with recently published work of Hu et al. [48] that measured flame speed of methane/air mixtures at elevated preheating temperature (T = 443 K) higher values compared with GRI Mech 3.0 model prediction, especially in the fuel rich side. Thus, the simulation results presented below for elevated reactant temperatures should be considered primarily as indicators of the general influence of the preheating. The simulations reveal that S_u increases with the temperature; as this one rises from room temperature to 477 K,

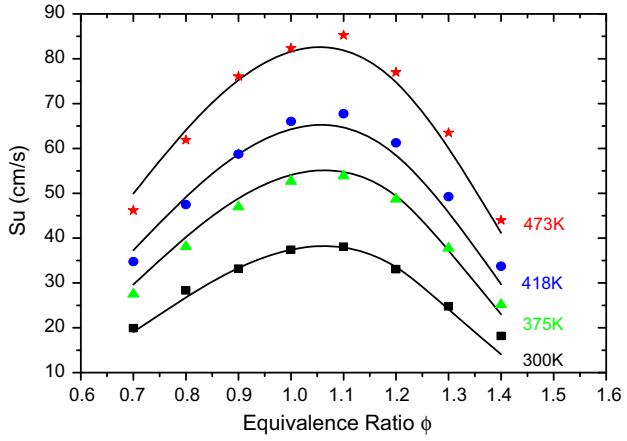

Fig. 10. Laminar flame speed variation versus equivalence ratio for different preheat temperatures (CH_4/air mixture, P = 0.1 MPa), (symbols represent experimental data; lines are numerical prediction of GRI-Mech 3.0 mechanism).

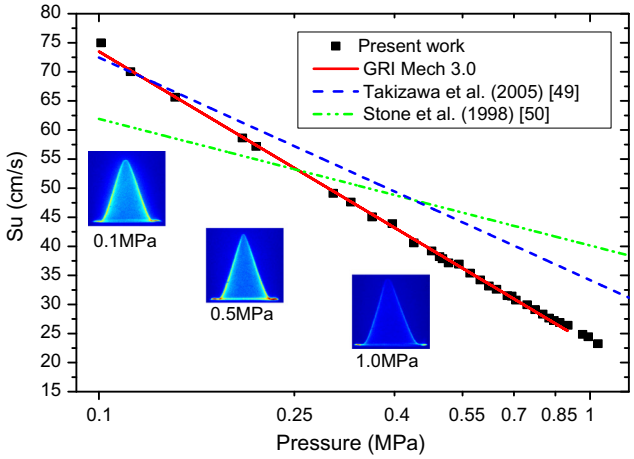

Fig. 11. Laminar flame speed variation versus pressure (CH_4/air mixture, T = 473 K, φ = 1.2). Symbols represent the experiments; solid line displays the numerical predictions of the GRI-Mech 3.0 mechanism and dashed lines represent the results of [49,50].

the flame speed increases by a factor of 2–2.5 for the range of equivalence ratios studied.

5.2.5. Pressure effect

Laminar flame speeds of methane/air are measured for a pressure range from 0.1–1.0 MPa in order to validate the accuracy of the system in elevated pressure conditions. The preheating temperature is fixed at 473 K and the equivalence ratio is maintained at 1.2. The pressure influence on the laminar flame speed of methane/air mixture is depicted in logarithmic coordinates in Fig. 11. As there are no experimental results in literature for these operating conditions, the current experimental results are compared with theoretical evolutions of the laminar flame speed calculated with the formalisms proposed by Takizawa et al. [49] and Stone et al.'s work [50] and with numerical results using the GRI-Mech 3.0 mechanism. Current experimental results are in better agreement with simulation results. A slightly overestimated flame speed is observed compared with simulation results in lower pressure from 0.1 to 0.2 MPa and a satisfied accordance in higher pressure from 0.2 to 1.0 MPa. The GRI-Mech 3.0 simulation is in excellent agreement with the experimental results over the major part of the pressure range that is investigated. As displayed in Fig. 11, the evolution of the methane/air flame speed in function of the pressure is interpolated using the classical power-law:

$$S_u = S_{u0}(P/P_0)^{\beta} \quad (7)$$

where S_{u0} is the flame speed at reference conditions (P_0 = 0.1 MPa, T_0 = 473 K, φ = 1.2). The power exponent β is deduced from the experimental results of Fig. 11 and for these experimental conditions its value is: −0.4557, which is quite approaching to recent investigation of Goswami et al.'s work [30] (β = −0.417 at φ = 1.2 and 298 K) using a heat flux burner for CH_4/air laminar flame speed measurements at elevated pressure (0.1–0.5 MPa). The parameter β is a function of the overall reaction order, n, (β = n/2−1), that is generally lower than 1.5 for hydrocarbons [21]. This result brings confidence in the validity of the method to determine flame speed at elevated pressure.

All these preliminary results have shown the good ability of the experimental device and of the images post-processing to accurately measure the laminar flame speed. In the second part of this study, the high-pressure Bunsen burner is used to characterize acetone/air flames.

5.3. Acetone/air mixtures

5.3.1. Equivalence ratio and preheating temperature effects

First of all, the flame speed, $S_{u0}(\varphi)$, is deduced at reference conditions (373 K, 0.1 MPa) from results presented in Fig. 12. The influence of the equivalence ratio on the flame speed is well described by the polynomial relation detailed above (see Eq. (4)) and the parameters $S_{u_{0,i}}$ are presented in Table 3.

In order to illustrate the preheat temperature effect on the acetone/air laminar flame speed, experimental measurements are performed at different temperatures: 373 K, 403 K, 443 K, 468 K and 523 K. Experimental and numerical results, obtained with the detailed reaction mechanism of Chong [4], are compared in Fig. 12 and firstly, the regular temperature effect is observed: flame speed increases with initial temperature of the fuel/air mixture. As can be seen, the predictions agree very well with the entire body of experimental data excepted in the rich side for T = 443 K in which small deviations are observed. For T = 523 K, discrepancies of ~5 cm/s are observed in the rich side.

To further illustrate the temperature dependence on the laminar flame speed, the evolution of the laminar flame speed recorded at atmospheric pressure is presented in a log-log graph (Fig. 13). For each equivalence ratio, the laminar flame speed increases nearly logarithmically with temperature (as indicated by the curve fits inthe figure). The power exponent α (φ) is determined from these results; values of α (φ) are listed in Table 4 and they are plotted versus equivalence ratio in Fig. 14. As shown in this figure, the evolution of the coefficient α with equivalence ratio follows an inverted bell-shaped curvature with a minimum value around φ = 1.05. The simulations carried out with the model of Chong [4]agree very well with the experiments over the whole range in equivalence ratio, except for rich mixtures (φ = 1.3). Similar behavior of coefficient α variation versus equivalence ratio was also observed as an inverted bell-shaped curvature in the work of Nilson et al. [7]. By fitting experimental data α (φ) with a third-order polynomial law (Eq. (5)) in Fig. 14, the equivalence ratio dependence coefficients α_i are then calculated and are summarized in Table 3.

5.3.2. Pressure effect

To analyze the apparent pressure dependence, measured laminar flame speed of acetone/air mixture at various equivalence ratios were first plotted as shown in Fig. 15. For comparison, the COSILAB prediction with the detailed reaction mechanism of

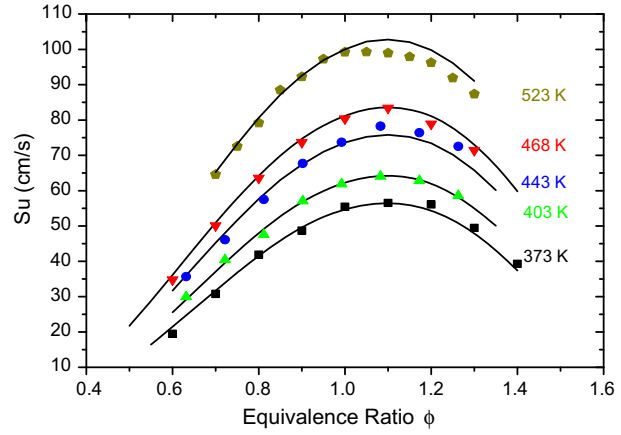

Fig. 12. Evolution of the laminar flame speed versus equivalence ratio for different preheat temperatures (acetone/air mixture, P = 0.1 MPa). Symbols represent experimental data; lines are numerical results using Chong's mechanism.

Table 3
Correlation parameters α_i, β_i and $S_{u_0,i}$ used in Eqs. (3), (4) and (5) (for acetone/air mixtures).

α_0	1.73	β_1	−0.318	$S_{u_0,\varphi=1}$	54.8
α_1	−0.44	β_2	0.215	$S_{u_0,1}$	39.4
α_2	2.01	β_3	−0.329	$S_{u_0,2}$	−161.9
α_3	−0.50			$S_{u_0,3}$	−91.4
				$S_{u_0,4}$	14.4

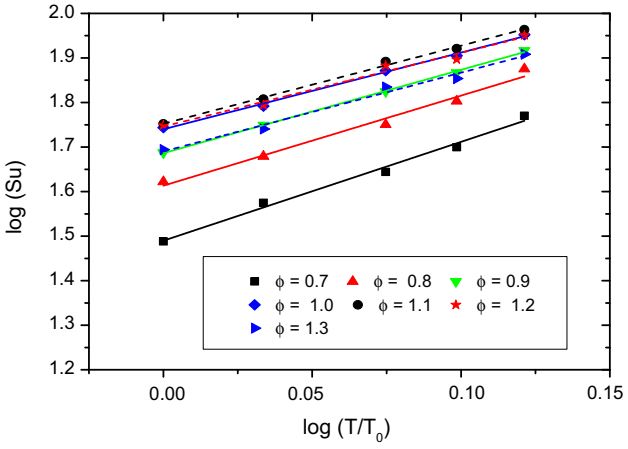

Fig. 13. Evolution of the laminar flame speed versus log (T/T_0) for different equivalence ratios (acetone/air mixture, P = 0.1 MPa). Lines represent the results of the correlation proposed in this study.

Chong [4] has been included. As opposed to the conclusions observed with the temperature effect, the laminar flame speed decreases with pressure whatever the selected equivalence ratio. On logarithmic scale, the power-law pressure dependence expressed in Eq. (3) is a straight line; this trend is observed in Fig. 15 for all equivalence ratios with minor deviations, particularly in the case of equivalence ratio of 0.9 for pressures above 0.25 MPa, where the evolution of the laminar flame speed is slightly curved in shape. Numerical predictions globally match the experimental data for each equivalence ratio.

According to the procedure used to determine the temperature dependence coefficients, the pressure dependence coefficients are then deduced from the evolution of the laminar flame speeds with pressure plotted in Fig. 16 on logarithmic scale. The resulting power exponents β(φ) are listed in Table 4 in function of the equivalence ratio and they are also compared in Fig. 17 with the corresponding power exponents derived using the kinetic model of Chong [4]. To the authors' knowledge, no empirical values of β (φ) are available in the literature for these experimental conditions.

As observed in Fig. 17, both the pressure power exponents show parabola-like variation with equivalence ratio from lean to moderately rich mixtures. The differences between the current experimental data and calculations are minor in the lean side, increasing significantly towards moderately rich flames. These differences can be explained by the experimental difficulties to record images of stable and perfectly axisymmetric flames in the case of rich acetone/air mixtures. For rich flames, the parameters β (φ)

Table 4
Values of the power exponents α(φ) and β(φ); comparison between values resulting from experimental data and numerical simulation.

	Experimental data	Chong's mechanism		Experimental data	Chong's mechanism
$\alpha_{\varphi=0.7}$	2.259	2.098	$\beta_{\varphi=0.7}$	−0.403	−0.403
$\alpha_{\varphi=0.8}$	2.056	1.925	$\beta_{\varphi=0.8}$	−0.384	−0.362
$\alpha_{\varphi=0.9}$	1.902	1.804	$\beta_{\varphi=0.9}$	−0.356	−0.338
$\alpha_{\varphi=1.0}$	1.794	1.743	$\beta_{\varphi=1.0}$	−0.305	−0.329
$\alpha_{\varphi=1.1}$	1.730	1.728	$\beta_{\varphi=1.1}$	−0.288	−0.332
$\alpha_{\varphi=1.2}$	1.767	1.758	$\beta_{\varphi=1.2}$	−0.297	−0.354

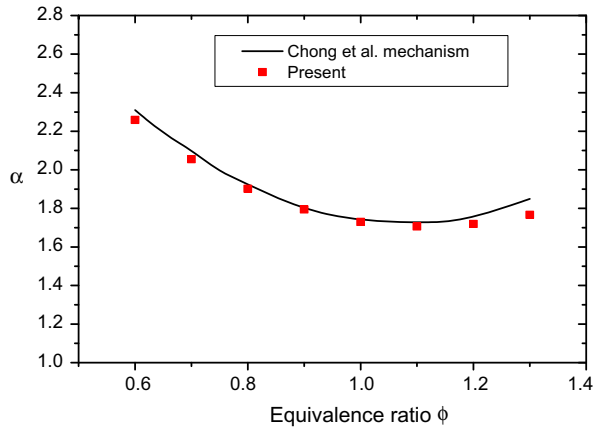

Fig. 14. Evolution of the power exponent α versus equivalence ratio (acetone/air mixture, P = 0.1 MPa).

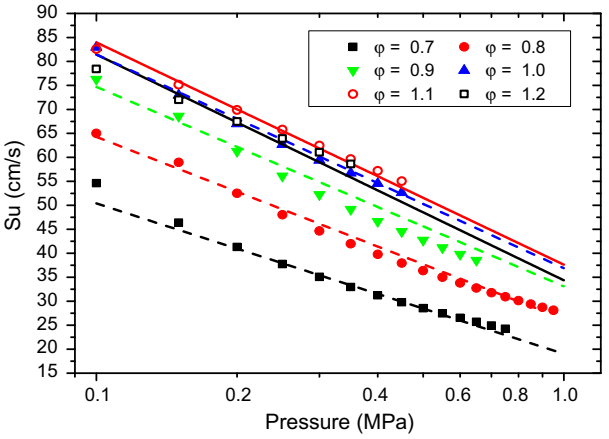

Fig. 15. Laminar flame speed versus pressure (acetone/air mixture, T = 473 K, φ = 0.7–1.2). Dash and solid lines are simulation results using Chong mechanism, symbols are experimental results.

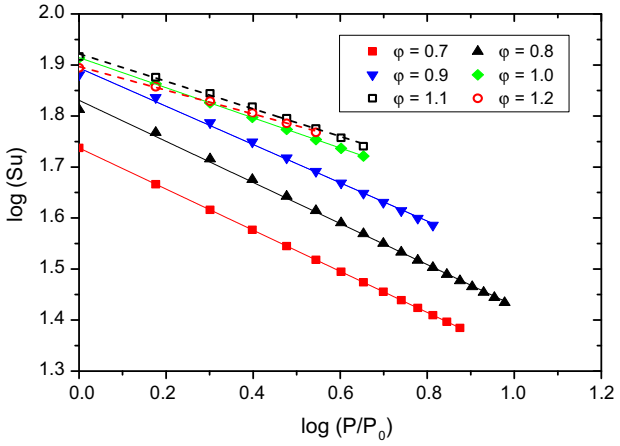

Fig. 16. Evolution of the laminar flame speed versus log P/P_0 for different equivalence ratios (acetone/air mixture, T = 473 K). Lines represent the results of the correlation proposed in this study.

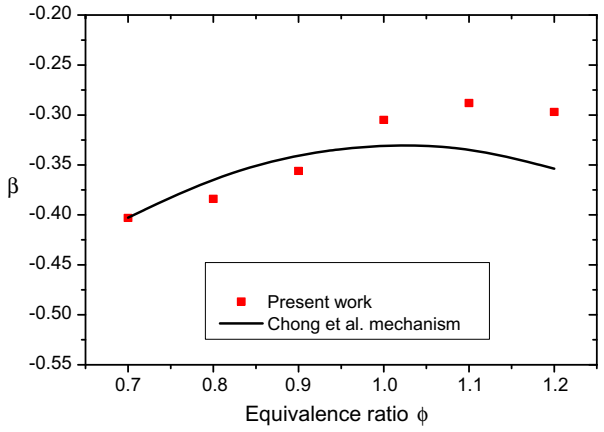

Fig. 17. Evolution of the power exponent β versus equivalence ratio (acetone/air mixture, T = 473 K).

are deduced from a more limited pressure range (0.1–0.45 MPa), that generates more uncertainties compared to the numerical simulation.

From the results of Fig. 17, the equivalence ratio effect on the power exponent β(φ) is observed by fitting with a second order polynomial law (Eq. (6)) the experimental data at different equivalence ratios; then the equivalence ratio dependence coefficients β_i can be deduced and are summarized in Table 3.

5.3.3. Correlation validation

The last objective of this study is to demonstrate the performance of the new laminar flame speed correlation for a wide range of pressure, temperature and equivalence ratio inthe case of acetone/air mixture. All the coefficients of the correlation determined by fitting our experimental results are listed in Table 3. Validity is ensured for ranges of equivalence ratio φ = [0.6–1.3], of temperature T = [373–523 K] and pressure up to 1 MPa. The overall accuracy of the correlation is shown in Fig. 18. The calculated flame speed $S_{u,corr}$ is reported with the experimental flame speed $S_{u,exp}$. The uncertainties of the correlation based from the 2σ intervals ($2 \times 1.65 = 3.3$ cm/s) of the residue $\Delta S_u = S_{u,exp} - S_{u,corr}$ are reported in Fig. 18 (dashed lines: ±σ). This can be compared to the experimental uncertainties evaluated in Section 3.2 of this study, varying from ±1 cm/s (at 300 K and 0.1 MPa) and close to ±4.5 cm/s (at 473 K, 0.35 MPa and φ = 1.2). These experimental uncertainties

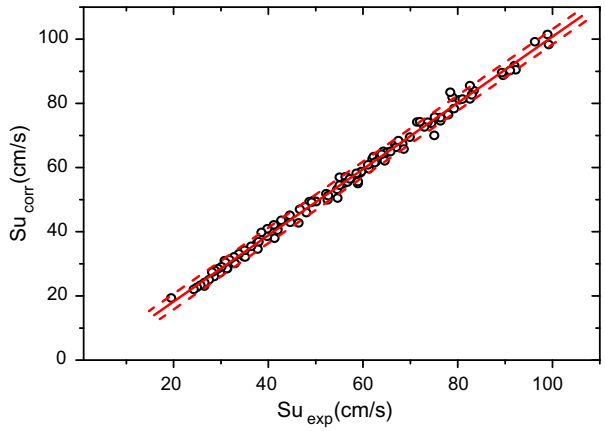

Fig. 18. Laminar flame speed obtained with the correlation expression compared to the experimental data. Dash lines indicate 2σ (σ = ±1.65 cm/s) uncertainties interval obtained from the residual ΔS_u distribution. Solid line corresponds to $S_{u,exp} = S_{u,corr}$.

are similar to the 2σ intervals of the correlation that demonstrates the reliability of the empirical correlation.

6. Conclusion

A new high-pressure laminar flame burner combined with a liquid fuel vaporization system has been designed for monitoring laminar flames of gaseous or liquid fuels over a wide range of operating conditions including preheat temperature, pressure and equivalence ratios. Based on the OH· chemiluminescence and OH-PLIF optical diagnostics for extracting the laminar burning velocity, experiments have been conducted to quantify the effects of pressure, reactant preheat temperature and equivalence ratio on various fuel/air mixtures. Methane fuel was firstly selected as a gaseous fuel to validate the operation of the high-pressure laminar Bunsen burner and to complement experimental data published in the open literature. Measurements were performed for pressures up to 1.0 MPa, preheat temperature ranging between 300 K and 523 K and equivalence ratio extending from 0.6 to 1.3. The methodology used to extract the laminar flame speed with OH· chemiluminescence signals has been specifically developed in the current work. This methodology requires the measurement of the flame surface area that has been detected from OH· images of the reaction zone. Particular attention has been paid to evaluate the effect of the flame thickness with pressure on the accuracy of the laminar flame speed. The resulted laminar flame speeds were also compared with those deduced from OH-PLIF optical measurements to evaluate the overall accuracy of the measurements. Typically, the accuracy of measurements which is obtained from the uncertainty of the calculated flame area and the repeatability of the experiments is ±1 cm/s at P = 0.1 MPa and T = 300 K and increases with preheat temperature and pressure (in case of rich flames particularly) to reach ±4.5 cm/s at P = 0.35 MPa, T = 473 K and φ = 1.2. Fundamental burning velocities of methane/air mixtures were compared with numerical predictions obtained with the GRI Mech 3.0 detailed kinetic mechanism and with published data. Whatever the pressure and preheat temperature investigated, a globally good agreement is obtained between our experimental results and GRI Mech 3.0 prediction.

The experimental work was extended to the measurements of laminar flame speed of acetone/mixtures at operating conditions identical to the ones used for methane/air mixtures. The experiments were also complemented and compared with numerical simulations conducted with Cosilab commercial software package using the published detailed chemical kinetic mechanism of

Chong and Hochgreb [4] for proposing a correlation relationship of the acetone/air laminar flame speed with pressure, preheat temperature and equivalence ratio. The effect of pressure and the preheat temperature on the burning velocity of acetone/air mixtures was interpreted using the general correlation $S_u = S_{u0}(\varphi)(T/T_0)^{\alpha}(P/P_0)^{\beta}$ in which both power exponents are depending on the equivalence ratio. Comparison between the experimental power exponents α (for temperature dependence) and β (for pressure dependence) and derived from the kinetic mechanism provides an independent and efficient tool for model validation and analysis.

References

[1] Dong C, Zhou Q, Zhao Q, Zhang Y, Xu T, Hui S. Experimental study on the laminar flame speed of hydrogen/carbon monoxide/air mixtures. Fuel 2009;88:1858–63.
[2] Wang Z, Weng W, He Y, Li Z, Cen K. Effect of H2/CO ratio and N2/CO2 dilution rate on laminar burning velocity of syngas investigated by direct measurement and simulation. Fuel 2015;141:285–92.
[3] Bosschaart K, de Goey L. Detailed analysis of the heat flux method for measuring burning velocities. Combust Flame 2003;132:170–80.
[4] Chong CT, Hochgreb S. Measurements of laminar flame speeds of acetone/methane/air mixtures. Combust Flame 2011;158:490–500.
[5] Bardin ME, Ivanov EV, Nilsson EJK, Vinokurov VA, Konnov AA. Laminar burning velocities of dimethyl carbonate with air. Energy Fuels 2013;27:5513–7.
[6] Burluka A, Harker M, Osman H, Sheppard C, Konnov A. Laminar burning velocities of three C3H6O isomers at atmospheric pressure. Fuel 2010;89:2864–72.
[7] Nilsson E, de Goey L, Konnov A. Laminar burning velocities of acetone in air at room and elevated temperatures. Fuel 2013;105. 496-02.
[8] Pichon S, Black G, Chaumeix N, Yahyaoui M, Simmie J, Curran H, et al. The combustion chemistry of a fuel tracer: measured flame speeds and ignition delays and a detailed chemical kinetic model for the oxidation of acetone. Combust Flame 2009;156. 494-04.
[9] Mol'kov V, Nekrasov V. Normal propagation velocity of acetone-air flames versus pressure and temperature. Combust, Explos Shock Waves 1981;17:280–3.
[10] Black G, Pichon S, Currant H, Simmie J, Donohue R, Chaumeix D. An experimental and modeling study of the combustion of acetone. In: Third European Combustion Meeting 2007, Greece.
[11] Yu G, Law C, Wu C. Laminar flame speeds of hydrocarbon + air mixtures with hydrogen addition. Combust Flame 1986;63:339–47.
[12] Lefkowitz JK, Won SH, Fenard Y, Ju Y. Uncertainty assessment of species measurements in acetone counterflow diffusion flames. Proc Combust Inst 2013;34:813–20.
[13] Jomaas G, Zheng X, Zhu D, Law C. Experimental determination of counterflow ignition temperatures and laminar flame speeds of C2–C3 hydrocarbons at atmospheric and elevated pressures. Proc Combust Inst 2005;30. 193-00.
[14] Smallbone A, Liu W, Law C, You X, Wang H. Experimental and modeling study of laminar flame speed and non-premixed counterflow ignition of n-heptane. Proc Combust Inst 2009;32:1245–52.
[15] Safer M, Tabet F, Ouadha A, Safer K. A numerical investigation of structure and emissions of oxygen-enriched syngas flame in counter-flow configuration. Int J Hydrogen Energy 2015;40:2890–8.
[16] Varea E, Modica V, Renou B, Boukhalfa AM. Pressure effects on laminar burning velocities and Markstein lengths for Isooctane–Ethanol–Air mixtures. Proc Combust Inst 2013;34:735–44.
[17] Jerzembeck S, Peters N, Pepiot-Desjardins P, Pitsch H. Laminar burning velocities at high pressure for primary reference fuels and gasoline: Experimental and numerical investigation. Combust Flame 2009;156. 292-01.
[18] Marshall S, Taylor S, Stone C, Davies T, Cracknell R. Laminar burning velocity measurements of liquid fuels at elevated pressures and temperatures with combustion residuals. Combust Flame 2011;158:1920–32.
[19] Galmiche B, Halter F, Foucher F. Effects of high pressure, high temperature and dilution on laminar burning velocities and Markstein lengths of iso-octane/air mixtures. Combust Flame 2012;159:3286–99.
[20] Beeckmann J, Cai L, Pitsch H. Experimental investigation of the laminar burning velocities of methanol, ethanol, n-propanol, and n-butanol at high pressure. Fuel 2014;117:340–50.
[21] Mannaa O, Mansour MS, Roberts WL, Chung SH. Laminar burning velocities at elevated pressures for gasoline and gasoline surrogates associated with RON. Combust Flame 2015;162:2311–21.
[22] Bouvet N, Chauveau C, Gökalp I, Lee S-Y, Santoro R. Characterization of syngas laminar flames using the Bunsen burner configuration. Int J Hydrogen Energy 2011;36. 992-05.
[23] Burbano HJ, Pareja J, Amell AA. Laminar burning velocities and flame stability analysis of syngas mixtures at sub-atmospheric pressures. Int J Hydrogen Energy 2011;36:3243–52.
[24] Garca-Soriano G, Castillo JL, Higuera FJ, Garca-Ybarra PL. Local burning velocity in a Bunsen jet flame. CR Mec 2012;340:789–96.
[25] Mazas A, Fiorina B, Lacoste D, Schuller T. Effects of water vapor addition on the laminar burning velocity of oxygen-enriched methane flames. Combust Flame 2011;158:2428–40.
[26] Natarajan J, Lieuwen T, Seitzman J. Laminar flame speeds of H2/CO mixtures: effect of CO2 dilution, preheat temperature, and pressure. Combust Flame 2007;151:104–19.
[27] Wang J, Wei Z, Yu S, Jin W, Xie Y, Zhang M, et al. Effects of stretch and preferential diffusion on tip opening of laminar premixed Bunsen flames of syngas/air mixtures. Fuel 2015;148:1–8.
[28] Gao X, Zhang Y, Adusumilli S, Seitzman J, Sun W, Ombrello T, et al. The effect of ozone addition on laminar flame speed. Combust Flame 2015;162:3914–24.
[29] Goswami M, Bastiaans R, Konnov A, de Goey L. Laminar burning velocity of lean H2-O mixtures at elevated pressure using the heat flux method. Int J Hydrogen Energy 2014;39:1485–98.
[30] Goswami M, Derks SC, Kris Coumans WJS, Oliveira MHA, Bastiaans RJ, Luijten CCM, Philipus AAKL, de Goey H. The effect of elevated pressure on the laminar burning velocity of methane+air mixtures. Combust Flame 2013;160:1627–35.
[31] Selle L, Poinsot T, Ferret B. Experimental and numerical study of the accuracy of flame-speed measurements for methane/air combustion in a slot burner. Combust Flame 2011;158:146–54.
[32] Sun S, Meng S, Zhao Y, Xu H, Guo Y, Qin Y. Experimental and theoretical studies of laminar flame speed of CO/H2 in O2/H2O atmosphere. Int J Hydrogen Energy 2016;41:3272–83.
[33] Walsh KT, Long MB, Tanoff MA, Smooke DM. Experimental and computational study of CH, CH·, and OH· in an axisymmetric laminar diffusion flame. Symp Int Combust 1998;1:615–23.
[34] Law C, Sung C. Structure, aerodynamics, and geometry of premixed flamelets. Pro Combust Inst 2000;26. 459-05.
[35] Kochar YN. Laminar flame speed and stretch sensitivity of hydrocarbon fuels at high preheat pressure and vitiation PhD thesis report. Georgia Institute of Technology; 2014.
[36] Smith G, Golden D, Frenklach M, Moriarty N, Eiteneer B, Goldenberg M et al. GRI-Mech Homepage. Gas Research Institute; 1999.
[37] Konnov A, Meuwissen R, de Goey L. The temperature dependence of the laminar burning velocity of ethanol flames. Proc Combust Inst 2011;33:1011–9.
[38] Metghalchi M, Keck JC. Burning velocities of mixtures of air with methanol, isooctane, and indolene at high pressure and temperature. Combust Flame 1982;48. 191-10.
[39] Agnew J, Graiff L. The pressure dependence of laminar burning velocity by the spherical bomb method. Combust Flame 1961;5:209–19.
[40] Smith D, Agnew JT. The effect of pressure on the laminar burning velocity of methane-oxygen-nitrogen mixtures. Symp Int Combust 1957;6:83–8.
[41] Gülder ÖL. Laminar burning velocities of methanol, ethanol and isooctane-air mixtures. Symp Int Combust 1982;19:275–81.
[42] Taylor SC. Burning velocity and the influence of flame stretch; 1991.
[43] Gu X, Haq M, Lawes M, Woolley R. Laminar burning velocity and Markstein lengths of methane–air mixtures. Combust Flame 2000;121:41–58.
[44] Halter F, Chauveau C, Djebaïli-Chaumeix N, Gökalp I. Characterization of the effects of pressure and hydrogen concentration on laminar burning velocities of methane–hydrogen–air mixtures. Proc Combust Inst 2005;30:201–8.
[45] Tahtouh T, Halter F, Mounaïm-Rousselle C. Measurement of laminar burning speeds and Markstein lengths using a novel methodology. Combust Flame 2009;156:1735–43.
[46] Huang Y, Sung C, Eng J. Laminar flame speeds of primary reference fuels and reformer gas mixtures. Combust Flame 2004;139:239–51.
[47] Bosschaart K, de Goey L. The laminar burning velocity of flames propagating in mixtures of hydrocarbons and air measured with the heat flux method. Combust Flame 2004;136:261–694.
[48] Hu E, Li X, Meng X, Chen Y, Cheng Y, Xie Y, et al. Laminar flame speeds and ignition delay times of methane–air mixtures at elevated temperatures and pressures. Fuel 2015;158:1–10.
[49] Takizawa K, Takahashi A, Tokuhashi K, Kondo S, Sekiya A. Burning velocity measurement of fluorinated compounds by the spherical-vessel method. Combust Flame 2005;141. 298-07.
[50] Stone R, Clarke A, Beckwith P. Correlations for the laminar-burning velocity of methane/diluent/air mixtures obtained in free-fall experiments. Combust Flame 1998;114:546–55.
[51] Dagaut P, Cathonnet M. The ignition, oxidation, and combustion of kerosene: a review of experimental and kinetic modeling. Pro Combust Inst 2006;32:48–92.
[52] He Y, Wang Z, Yang L, Whiddon R, Li Z, Zhou J, et al. Investigation of laminar flame speeds of typical syngas using laser based Bunsen method and kinetic simulation. Fuel 2012;95:206–13.
[53] Fu J, Tang C, Jin W, Thi LD, Huang Z, Zhang Y. Study on laminar flame speed and flame structure of syngas with varied compositions using OH-PLIF and spectrograph. Int J Hydrogen Energy 2013;38:1636–43.
[54] Lapalme D, Seers P. Influence of CO2, CH4, and initial temperature on H2/CO laminar flame speed. Int J Hydrogen Energy 2014;39:3477–86.
[55] Hu X, Yu Q, Liu J, Sun N. Investigation of laminar flame speeds of CH4/O2/CO2 mixtures at ordinary pressure and kinetic simulation. Energy 2014;70:626–34.